iScience

CellPress
OPEN ACCESS

Article

cGAS-STING activation contributes to podocyte injury in diabetic kidney disease

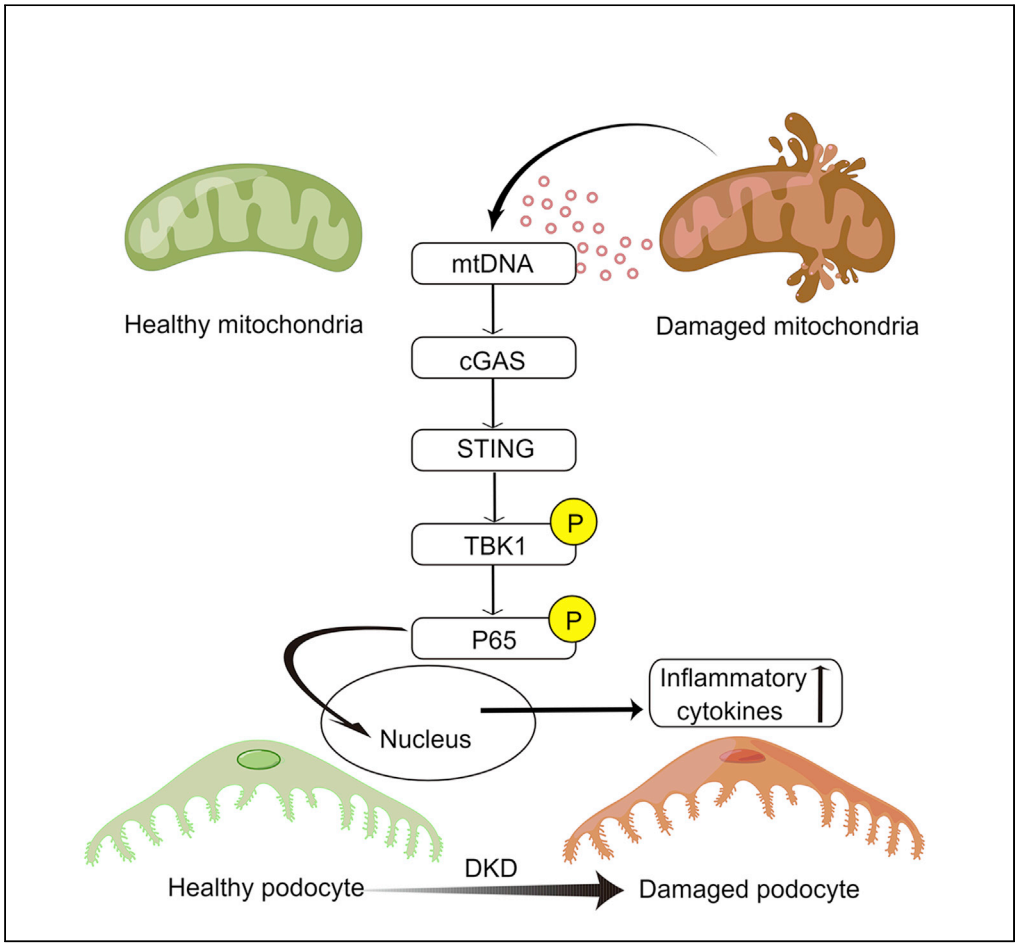

Nan Zang, Chen Cui, Xinghong Guo, ..., Zheng Sun, Chuan Wang, Li Chen

201562008239@email.sdu.edu.cn (C.W.)
chenli3@email.sdu.edu.cn (L.C.)

Highlights

Cytosolic mitochondrial DNA activates cGAS-STING signaling in podocyte

cGAS-STING activation induces podocyte injury in diabetic and obese mice

Inhibition of STING ameliorates podocyte injury in diabetic and obese mice

Zang et al., iScience *25*, 105145
October 21, 2022
https://doi.org/10.1016/j.isci.2022.105145

iScience

CellPress
OPEN ACCESS

Article

cGAS-STING activation contributes to podocyte injury in diabetic kidney disease

Nan Zang,[1,6] Chen Cui,[1] Xinghong Guo,[1] Jia Song,[1] Huiqing Hu,[1] Mengmeng Yang,[1] Mingyue Xu,[1] Lingshu Wang,[1,2,3,4] Xinguo Hou,[1,2,3,4] Qin He,[1,2,3,4] Zheng Sun,[5] Chuan Wang,[1,2,3,4,*] and Li Chen[1,2,3,4,*]

SUMMARY

Diabetic kidney disease (DKD) is the leading cause of end-stage renal diseases. DKD does not have efficacious treatment. The cGAS-STING pathway is activated in podocytes at the early stage of kidney dysfunction, which is associated with the activation of STING downstream effectors TBK1 and NF-κB but not IRF3. Lipotoxicity induces mitochondrial damage and mtDNA leakage to the cytosol through Bcl-2 associated X protein (BAX) in podocytes. BAX-mediated mtDNA cytosolic leakage can activate the cGAS-STING pathway in the absence of lipotoxicity and is sufficient to cause podocyte injury. Depletion of cytosolic mtDNA, genetic STING knockdown, or pharmacological inhibition of STING or TBK1 alleviates podocyte injury and improves renal functions in cultured podocytes or mouse models of diabetes and obesity. These results suggest that the mtDNA-cGAS-STING pathway promotes podocyte injury and is a potential therapeutic target for DKD or other obesity-related kidney diseases.

INTRODUCTION

Diabetic kidney disease (DKD) is a life-threatening complication of diabetes mellitus and the leading cause of end-stage renal diseases, without efficacious treatment (Van Buren and Toto, 2013). The common early hallmark of DKD is albuminuria (Perkins et al., 2003) and pathological kidney features, including the aggregation of the extracellular matrix, thickening of glomerular basement membrane (GBM), and progressive loss of podocytes (Ziyadeh et al., 2000; Ziyadeh, 2004; Najafian et al., 2011). Recent studies have found that podocyte injury plays a central role in the development of DKD (Dai et al., 2017). Podocytes are highly specialized epithelial cells of the glomerulus, lining the lateral side of the GBM (Pavenstadt et al., 2003). One of the earliest abnormalities in the development of DKD is podocyte injury (Menini et al., 2007), which contributes to the breakdown of the glomerular filtration barrier, albuminuria, and the deterioration of renal function (Greka and Mundel, 2012).

Emerging studies find that DKD is a chronic inflammatory disease (Hickey and Martin, 2018; Navarro-Gonzalez et al., 2011). The cyclic GMP-AMP (cGAMP) synthase (cGAS) and stimulator of interferon genes (STING) pathway is a critical player in metabolic inflammation (Bai and Liu, 2019). cGAS serves as a sensor of dsDNA aberrantly localized in the cytosol independent of its sequence context (Zhang et al., 2014). Activated cGAS induces the production of 2′3′-cGAMP, a cyclic dinucleotide composed of adenosine and guanosine linked via two phosphodiester linkages, which binds to the ER(ER)-localized STING (Chen et al., 2016). The STING then translocates from the ER to perinuclear structures. During the trafficking process, STING recruits and activates TANK binding kinase1 (TBK1), which phosphorylates interferon regulatory factor 3 (IRF3) and nuclear factor-kB (NF-kB), leading to the production of type 1 interferons (IFNs) and other inflammatory cytokines, respectively (Tanaka and Chen, 2012). And during the cGAS-STING activation, the increase of protein levels of cGAS and STING is a common phenomenon (Wang et al., 2020). The *in vivo* function of cGAS-STING in DKD is unclear.

Here, we use mouse models of diabetes and obesity to study the pathogenic role of STING-dependent inflammation in podocytes. Our results show that mtDNA leakage occurs in podocytes and activates the cGAS-STING pathway during the early stage of DKD, which is associated with the activation of downstream TBK1 and NF-κB p65 but not IRF3, leading to inflammation and podocyte injury. The function of

[1]Department of Endocrinology, Qilu Hospital, Cheeloo College of Medicine, Shandong University, Jinan, Shandong 250012, China

[2]Institute of Endocrine and Metabolic Diseases of Shandong University, Jinan, Shandong 250012, China

[3]Key Laboratory of Endocrine and Metabolic Diseases, Shandong Province Medicine and Health, Jinan, Shandong 250012, China

[4]Jinan Clinical Research Center for Endocrine and Metabolic Disease, Jinan, Shandong 250012, China

[5]Department of Medicine – Endocrinology, Baylor College of Medicine, Houston, TX, USA

[6]Lead contact

*Correspondence: 201562008239@email.sdu.edu.cn (C.W.), chenli3@email.sdu.edu.cn (L.C.)

https://doi.org/10.1016/j.isci.2022.105145

cGAS-STING in podocytes is cell-autonomous. Pharmacologic blocking of the cGAS-STING pathway is nephroprotective in mouse models of diabetes and obesity, demonstrating the therapeutic potential for DKD or other obesity-related kidney diseases.

RESULTS

Podocyte injury is a major early-stage manifestation of diabetic kidney disease

To investigate the time course of renal functional changes in db/db mice, we monitored diabetic db/db mice from 4 weeks old, using nondiabetic db/m mice as control. 10-week-old db/db mice showed higher body weight (Figure S1A) and fasting blood glucose (FBG) (Figure S1B), with dyslipidemia, impaired glucose tolerance, and insulin sensitivity compared to the control mice (Figures S1C-S1E). db/db mice started to show obvious microalbuminuria at 10 weeks old (Figure S1F), while the levels of blood urea nitrogen (BUN) and serum creatinine (Scr) were still normal at this age (Figure S1G). Histology analyses (Figures S1H and S1I) revealed obvious glomerular hypertrophy at the age of 10 weeks (Figures S1H and S1I) and slight mesangial expansion (Figure S1I), but without obvious collagen disposition (Figure S1I). Nephrin, a key protein of the slit diaphragm of podocytes, was reduced in db/db mice at 10 weeks old compared to control mice, indicating podocyte injury (Figure S1I). Ultrastructures of podocytes showed extensive fused foot processes and irregularly thickened GBM in db/db mice at 10 weeks old (Figure S1I), associated with increased podocyte apoptosis (Figures S1H and S1I). Therefore, 10 weeks old db/db mice are at the early stage of DKD, with podocyte injury as the main manifestation.

Activation of the cyclic GMP-AMP synthase-stimulator of interferon gene pathway precedes podocyte injury

Compared to the lean control mice, db/db mice showed an activated cGAS-STING pathway at about 8 weeks old in the renal cortex, mainly in glomerular podocytes (Figures 1A and S2A), in line with the urine protein and podocyte injury results. The cGAS and STING protein levels were elevated, accompanied by increased TBKI phosphorylation levels (Figure 1B). However, the levels of IRF3 phosphorylation or IFN-β remained unaltered (Figure 1B), suggesting that the cGAS-STING activation in db/db mice leads to selective downstream effectors in renal parenchymal cells.

Inhibition of the cyclic GMP-AMP synthase-stimulator of interferon gene pathway ameliorates podocyte injury in db/db mice

To address the role of the cGAS-STING pathway in renal dysfunction, we utilized C176, a pharmacological inhibitor of STING. Mice were administered with C176 from 7 weeks old for 21 consecutive days. C176 did not affect body weight (Figures S3A and S3B), glucose tolerance test, insulin tolerance test, or dyslipidemia (Figures S3C-S3E). C176 lowered FBG moderately after 21 days of treatment (Figure 2A). Interestingly, at the very first week of C176 treatment, microalbuminuria was significantly reduced (Figure 2B), without affecting the levels of BUN and Scr (Figure S3F). Glomerula hypertrophy (Figures 2C and 2D) and mesangial expansion were relieved after C176 treatment (Figure S3G) without collagen disposition (Figure S3G). C176 also rescued nephrin levels in db/db mice (Figure 2C) and alleviated podocyte apoptosis (Figures 2C and 2D). An orderly arrangement of podocytes, clear foot processes, and uniform glomerular basement membrane was observed in C176-treated db/db mice (Figure 2C). These changes were associated with blunted activation of cGAS and STING and its downstream TBK1 phosphorylation, while the levels of canonical phosphorylation of IRF3 and IFN-β remained unaltered. C176 also prevented the upregulation of cGAS/STING protein levels, suggesting that the protein level upregulation requires STING activity, probably in a feedback loop that is yet to be defined. (Figures 2E and 2F). Thus, the inhibition of the cGAS-STING pathway ameliorates podocyte injury in db/db mice.

Inhibition of the cyclic GMP-AMP synthase-stimulator of interferon gene pathway improves podocyte injury in diet-induced obesity mice

The genetic db/db mouse model is associated with severe obesity and high FBG. To address the role of cGAS-STING in a more modest obesity model, we used a diet-induced obesity (DIO) model fed with a high-fat diet (Figure 3A) (Sun et al., 2021). Activation of the cGAS-STING pathway occurred in DIO mice, especially in glomerular podocytes (Figures 3B and S2B). After high-fat diet for 16 weeks, DIO mice developed obesity (Figures 3C and S4A), abnormal glucose, and insulin tolerance (Figure S4B). C176 intervention decreased the body weight gain of DIO mice (Figure 3C), improved glucose tolerance and insulin tolerance (Figure S4B), and reduced FBG levels (Figure 3D). As DIO mice produced less urine compared with db/db mice, we used the urinary albumin creatinine

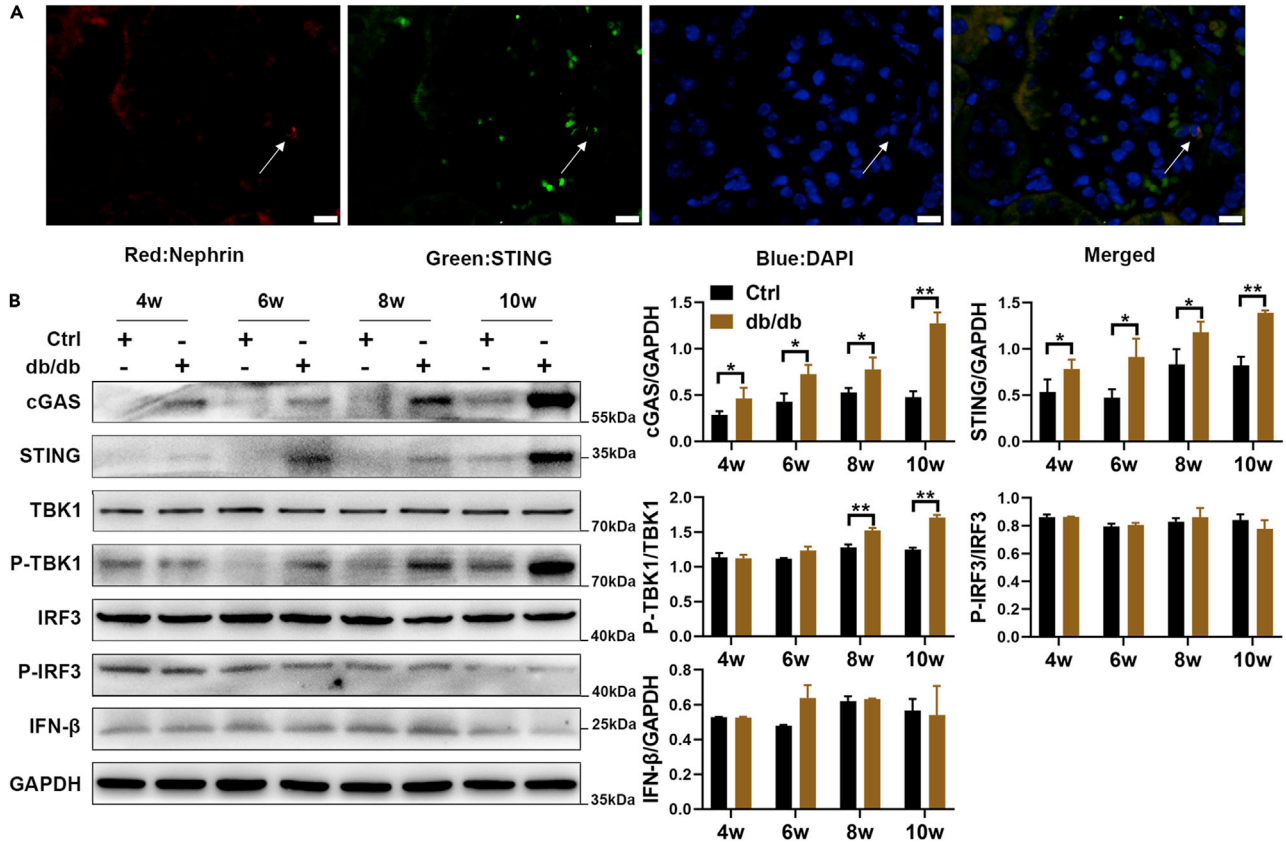

Figure 1. Activation of the cGAS-STING pathway precedes podocyte injury

(A) IF staining of nephrin, STING, and DAPI in db/db mice (scale bars, 10μm) (n = 3 male db/db mice).

(B) Western blot analysis of cGAS, STING, P-TBK1/TBK1, P-IRF3/IRF3, and IFNβ in kidney cortical tissue (n = 15 male db/db mice, n = 14 male control mice).

Data are mean ± SEM *p < 0.05, **p < 0.01, ***p < 0.001 with Student's *t* test. See also Figure S2.

ratio (ACR) to assess albuminuria. Increased ACR in DIO mice was decreased after C176 treatment (Figure 3E). Importantly, the C176-mediated improvement in ACR preceded its effect on FBG (Figures 3D and 3E), suggesting that the nephroprotective effect of C176 is not dependent on improved glucose homeostasis. Other manifestations of kidney injury in DIO mice include glomerular hypertrophy (Figures 3F and 3G) and mesangial expansion (Figure S4C) without fibration (Figure S4C). As for podocyte injury, DIO mice showed lower levels of nephrin, diffused thickening of GBM, reduced number of podocytes, and extensive fusion of foot processes (Figure 3G), increased apoptosis of podocyte (Figures 3F and 3G), elevated STING protein levels, and TBK1 phosphorylation in the renal cortex (Figures 3H and 3I). All of these manifestations of podocyte injury were improved after C176 treatment (Figures 3C-3I). These results demonstrate that the inhibition of the cGAS-STING pathway reduces albuminuria and improves podocyte injury in DIO mice.

Cyclic GMP-AMP synthase-stimulator of interferon gene activation mediates palmitic acid-induced podocyte injury

To address whether the protective effects of cGAS-STING inhibition on podocyte injury are cell-autonomous and to explore the underlying molecular mechanism, we used the MPC5 podocyte cell line. The cells were photographed by inverted phase-contrast microscopy and characterized by immunofluorescence for the podocyte markers WT-1, synaptopodin, and nephrin. (Figures S5A and S5B). We induced podocyte damage with palmitic acid (PA) because DKD and obesity-related kidney disease are characterized by elevated free fatty acids (FFAs) and podocytes are highly susceptible to saturated FFAs (Sieber et al., 2010, 2013). The dose of PA (250 μM) was based on physiologic concentrations of palmitate at 250 μM or higher in the serum of diabetic mice (Rumora et al., 2018). Upon PA treatment, the levels of nephrin and podocin, marker proteins of podocyte, were decreased (Figure 4A), while apoptosis increased (Figures 4A-4D), associated with increased inflammatory cytokines IL-6 and TNF-α (Figure 4E). The PA-induced podocyte injury was associated with cGAS-STING

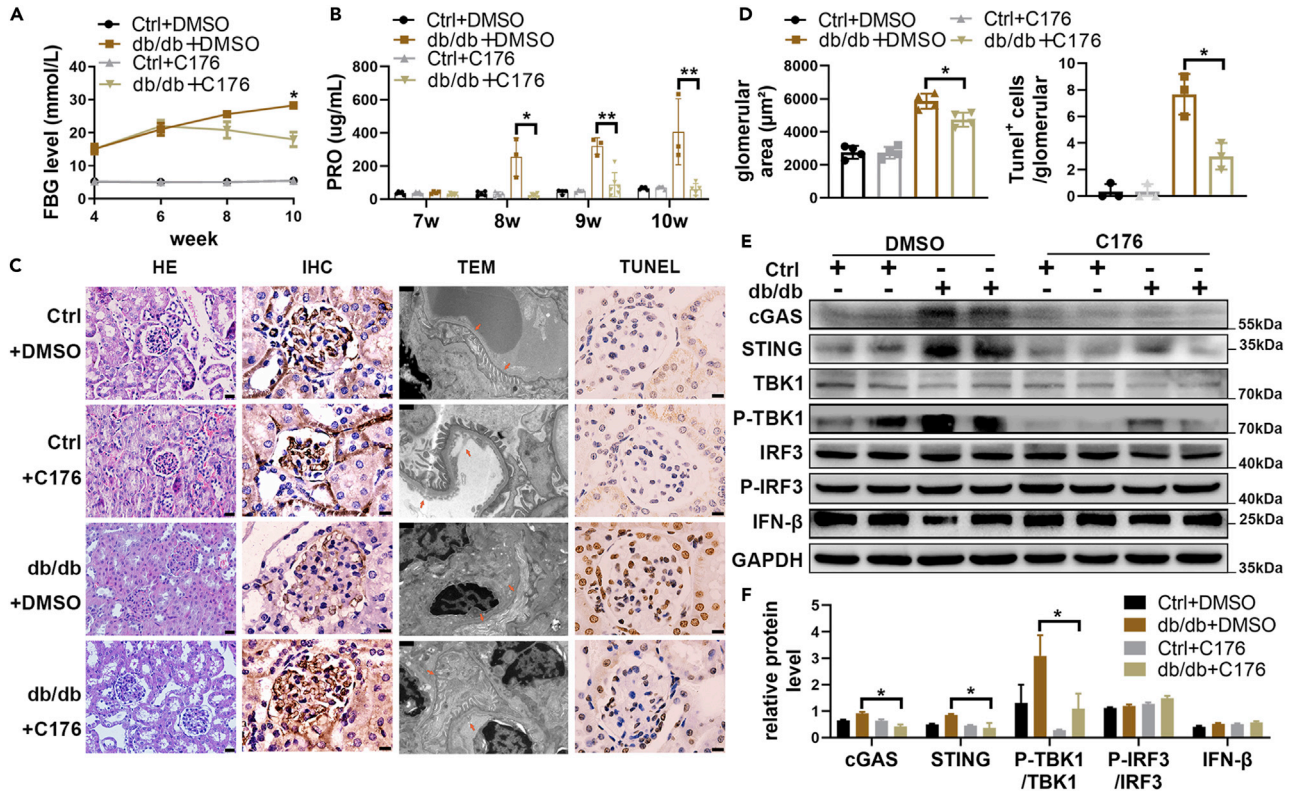

Figure 2. Inhibition of the cGAS-STING pathway ameliorates podocyte injury in db/db mice

(A) FBG levels of C176 or vehicle DMSO-treated mice at 10 weeks old after treatment for 3 weeks (db/db + C176, n = 6; db/db + DMSO, n = 3, db/m + C176, n = 5, db/m + DMSO, n = 5).

(B) The proteinuria (PRO).

(C and D) H&E staining (scale bars, 20μm), IHC staining of nephrin (scale bars, 10μm), TEM (scale bars, 0.6μm) and TUNEL staining (scale bars, 10μm) of kidney tissue in C176 or vehicle DMSO-treated mice (db/db + C176, n = 6; db/db + DMSO, n = 3, db/m + C176, n = 5, db/m + DMSO, n = 5).

(E and F) Western blot analysis of cGAS, STING, P-TBK1/TBK1, P-IRF3/IRF3 and IFNβ in kidney cortical tissue at 10 weeks old after C176 or vehicle DMSO treatment for 3 weeks (db/db + C176, n = 6; db/db + DMSO, n = 3, db/m + C176, n = 5, db/m + DMSO, n = 5). Data are mean ± SEM *p < 0.05, **p < 0.01, ***p < 0.001 with two-way ANOVA followed by Sidak post hoc test (B) and Kruskal-Wallis test (A, D, F). See also Figure S3.

activation, as estimated by increased levels of phosphorylation of the downstream molecules TBK1 and NF-kB p65 (Figures 4F and 4G). Also, in PA-induced podocytes, STING shifted to the perinuclear region and co-localized with cis-Golgi matrix protein 130 (GM130), a marker for the Golgi apparatus (Figure S6A). The cGAS and STING protein levels were also increased by PA. However, IRF3, another downstream molecule of the cGAS-STING pathway, was not phosphorylated, and the protein level of IFN-b remained unaltered (Figures 4F and 4G). This selective activation of downstream effectors is consistent with what we found in db/db or DIO mice.

Next, we investigated the impact of C176 on PA-induced podocyte injury in MPC5 cells. C176 (1 μM) ameliorated PA-induced podocyte injury, as determined by restored protein levels of nephrin and podocin (Figures 4H and 4I), reduced apoptosis (Figures 4H-4K), reduced TBK1 and NF-kB p65 phosphorylation reduced IL-6 and TNF-α levels (Figures 4L-4N). Specific knockdown of STING by small interfering RNA (siRNA) produced similar results (Figures 5A-5G), demonstrating cell-autonomous protective effects of STING inhibition in lipotoxicity-associated podocyte injury.

We further explored the downstream effectors of STING in podocyte injury. As TBK1 is a major downstream player in the cGAS-STING pathway, we assessed the effect of a TBK1 inhibitor GSK8612 (Thomson et al., 2019) on PA-induced podocyte injury. On top of PA treatment, GSK8612 increased nephrin and podocin levels (Figures 5H and 5I), decreased apoptosis (Figures 5H-5K), abrogated IL-6 and TNF-α production (Figure 5L), and reduced TBK1 and p65 phosphorylation (Figures 5M and 5N), suggesting that the inhibition of TBK1 is sufficient to generate cell-autonomous protective effects. Interestingly, GSK8612 increased STING protein levels under

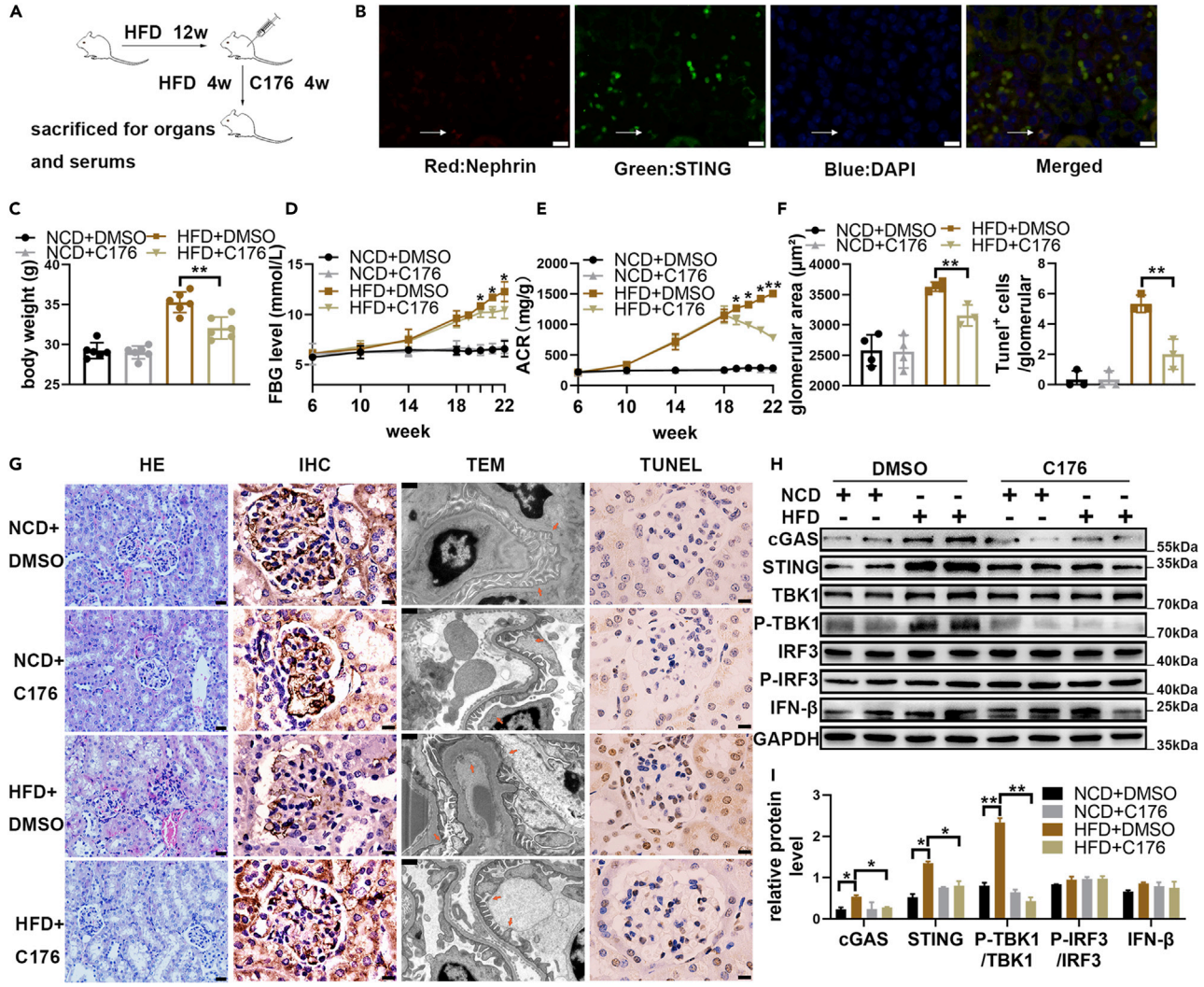

Figure 3. Inhibition of the cGAS-STING pathway improves podocyte injury in DIO mice

(A) Experimental design.

(B) IF staining of nephrin, STING, and DAPI in the kidney of DIO mice at 22 weeks old after feeding high-fat diet (HFD) for 16 weeks (Scale bars, 10μm).

(C) Body weight at 22 weeks old after feeding HFD for 16 weeks.

(D) FBG levels (HFD + C176, n = 6; HFD + DMSO, n = 6, NCD + C176, n = 6, NCD + DMSO, n = 6, male mice).

(E) Urine albumin-to-creatinine ratio (ACR).

(F and G) H&E staining (scale bars, 20μm), IHC staining of nephrin (scale bars, 10μm), TEM (scale bars, 0.6μm) and TUNEL staining (scale bars, 10μm) of kidney tissue (HFD + C176, n = 6; HFD + DMSO, n = 6, NCD + C176, n = 6, NCD + DMSO, n = 6, male mice).

(H-I) Western blot analysis of cGAS, STING, P-TBK1/TBK1, P-IRF3/IRF3 and IFNβ in kidney cortical tissue at 22 weeks old after feeding HFD for 16 weeks (HFD + C176, n = 6; HFD + DMSO, n = 6, NCD + C176, n = 6, NCD + DMSO, n = 6, male mice). Data are mean ± SEM *p < 0.05, **p < 0.01, ***p < 0.001 with Kruskal-Wallis test. See also Figures S2 and S4.

the baseline conditions in the absence of PA (Figures 5M and 5N), suggesting that TBK1 exerts a negative-feedback regulatory function on STING, probably through promoting STING ubiquitination and protein degradation (Zhao et al., 2018). In summary, our results show that the cGAS-STING activation mediates PA-induced podocyte injury, likely through TBK1.

Stimulator of interferon gene activation in podocytes is associated with mitochondrial damage

What activates the cGAS-STING pathway in podocytes in the context of obesity and diabetes? Recent studies suggest that mitochondrial damage and mtDNA leakage to the cytosol can activate the cGAS-STING pathway

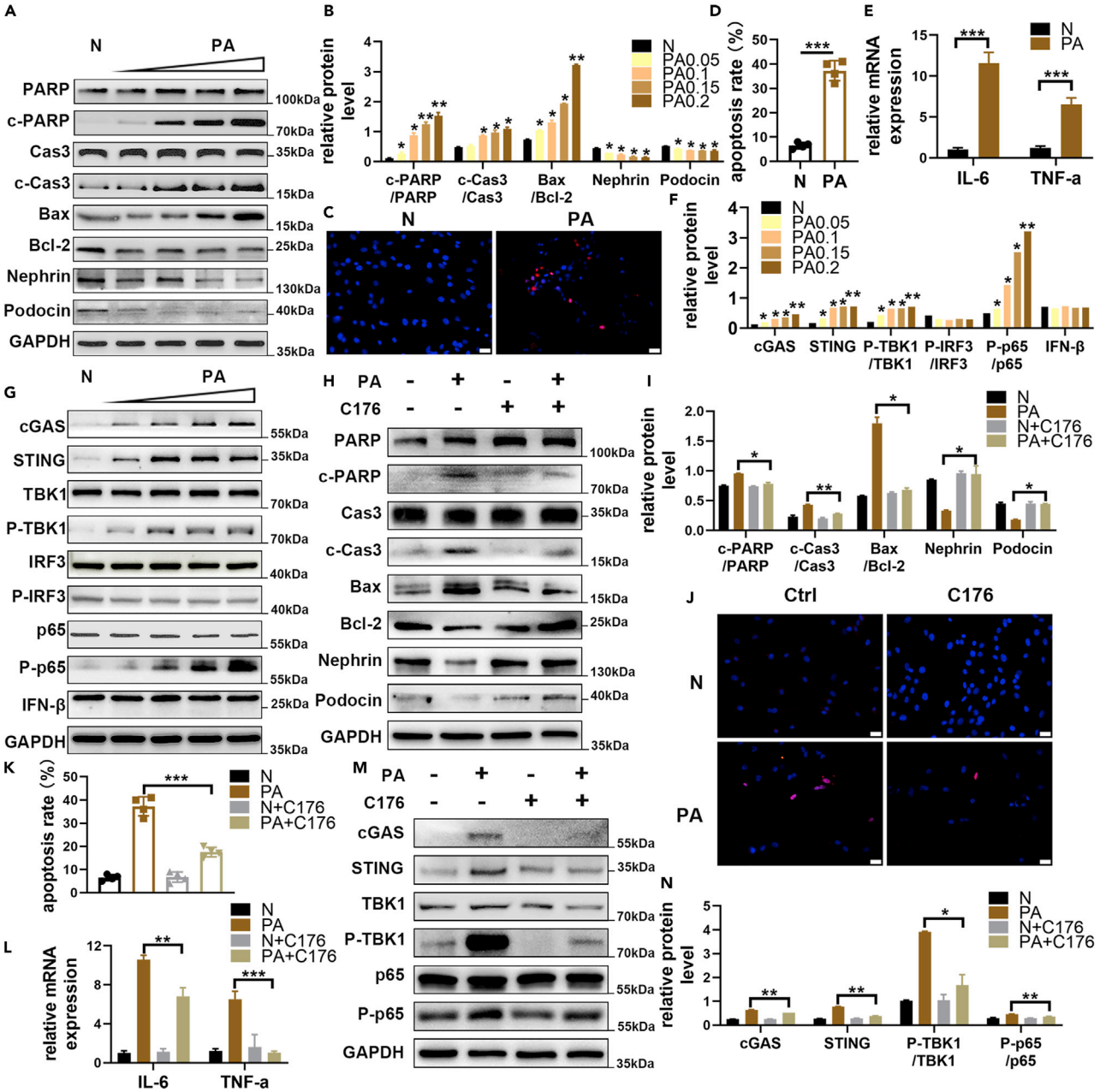

Figure 4. cGAS-STING activation mediates PA-induced podocyte injury

(A and B) Western blot analysis of Bax/Bcl-2, cleaved caspase3/caspase 3 (c-Cas3/Cas3), cleaved PARP/PARP (c-PARP/PARP), nephrin, and podocin in MPC5 cells stimulated by palmitic acid (PA, 0.25 mM for 8 h) (n = 6).

(C and D) TUNEL staining of PA-stimulated MPC5 cells (scale bars, 20μm).

(E) RT-qPCR analysis of mRNA levels of IL-6 and TNF-α in PA-stimulated MPC5 cells. (n = 6).

(F and G) Western blot analysis of cGAS, STING, P-TBK1/TBK1, P-IRF3/IRF3, P-p65/p65, and IFNβ in PA-stimulated MPC5 cells (n = 6).

(H and I) Western blot analysis of Bax/Bcl2, c-Cas3/Cas3, c-PARP/PARP, nephrin, and podocin in MPC5 cells following PA or/and C176 (1 μM) treatment. (n = 6).

(J and K) TUNEL staining of C176-treated MPC5 cells following PA treatment (scale bars, 20μm).

(L) RT-qPCR analysis of mRNA levels of IL-6 and TNF-α in C176-treated MPC5 cells following PA treatment (n = 6).

(M and N) Western blot analysis of cGAS, STING, P-TBK1/TBK1, and P-p65/p65 in C176-treated MPC5 cells following PA treatment (n = 6). Data are mean ± SEM *p < 0.05, **p < 0.01, ***p < 0.001 with Student's *t* test (D-E) and Kruskal-Wallis test (B, F, I, K-L, N). See also Figure S6.

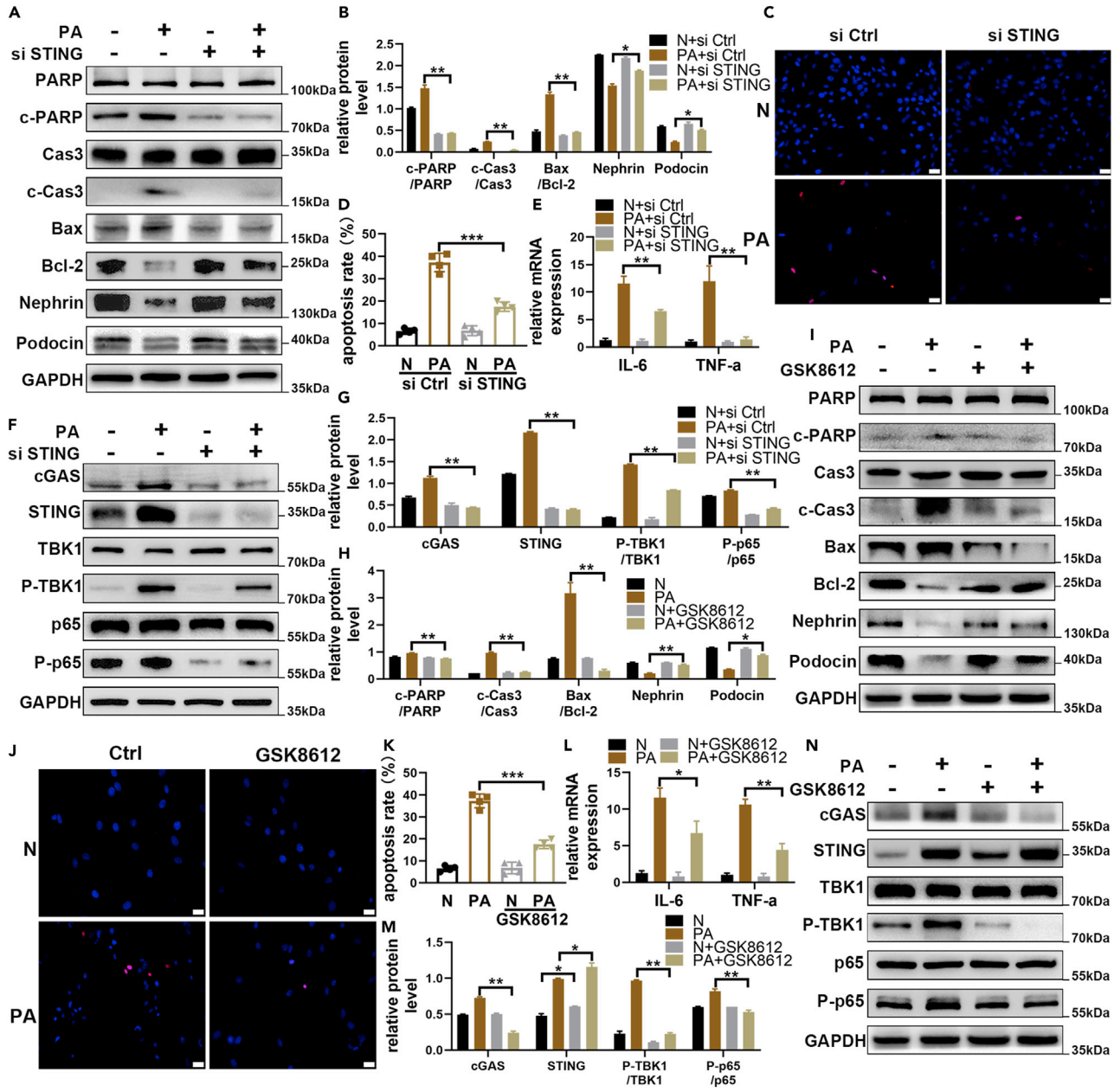

Figure 5. STING and TBK1 contribute to PA-induced podocyte injury

MPC5 cells were treated with siRNA of STING or TBK1 inhibitor, GSK8612 (5 μM).

(A and B) Western blot analysis of Bax/Bcl2, c-Cas3/Cas3, c-PARP/PARP, nephrin, and podocin in STING-knockdown MPC5 cells following PA stimulation (0.25 mM for 8 h) (n = 6).

(C and D) TUNEL staining of STING-knockdown MPC5 cells following PA treatment (scale bars, 20μm).

(E) RT-qPCR analysis of IL-6 and TNF-α in MPC5 cells (n = 6).

(F and G) Western blot analysis of cGAS, STING, P-TBK1/TBK1 and P-p65/p65 (n = 6).

(H and I) Western blot analysis of Bax/Bcl2, c-Cas3/Cas3, c-PARP/PARP, nephrin, and podocin in MPC5 cells after treatment with PA or/and a TBK1 inhibitor, GSK8612 (5 μM) (n = 6).

(J and K) TUNEL staining of GSK8612-treated MPC5 cells (scale bars, 20μm).

(L) RT-qPCR analysis of IL-6 and TNF-α in GSK8612-treated MPC5 cells following PA treatment (n = 6).

(M and N) Western blot analysis of cGAS, STING, P-TBK1/TBK1, and P-p65/p65 in MPC5 cells (n = 6). Data are mean ± SEM *p < 0.05, **p < 0.01, ***p < 0.001 with Kruskal-Wallis test.

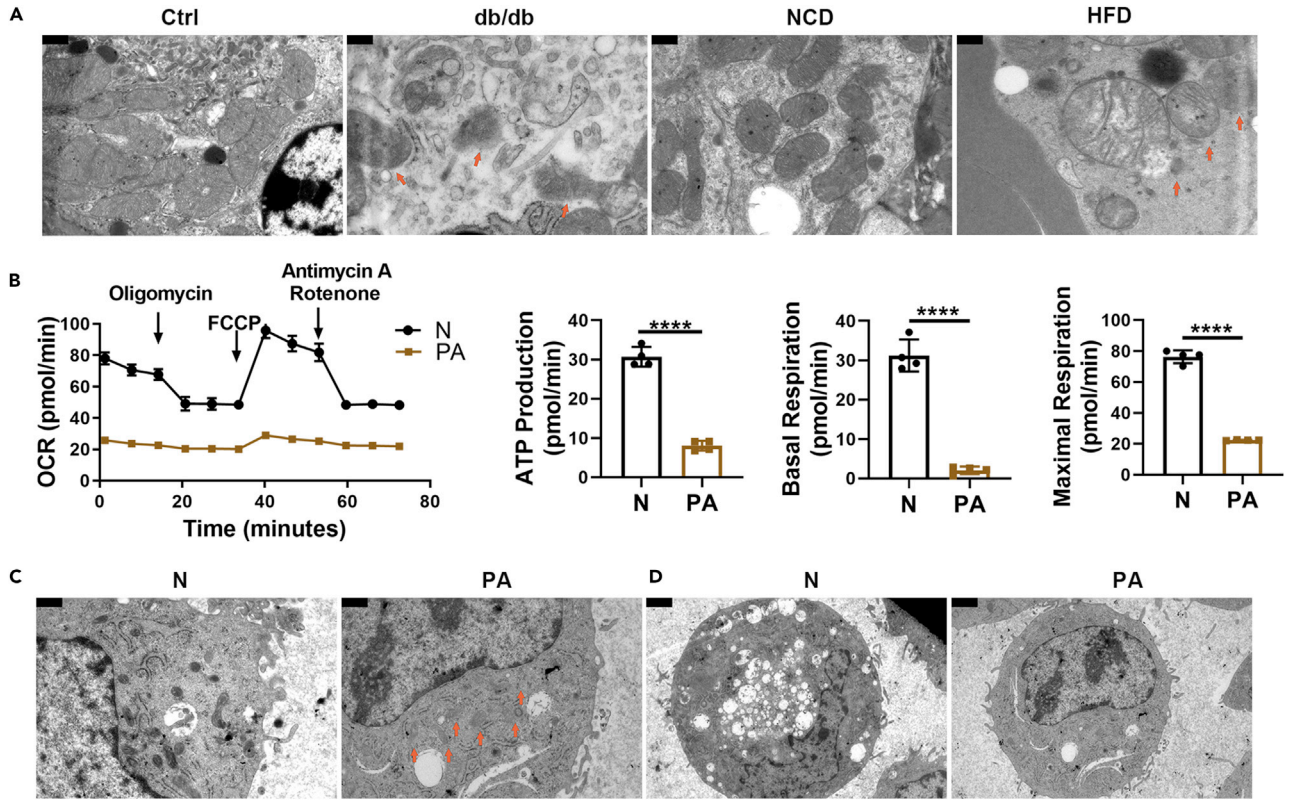

Figure 6. STING activation in podocytes is associated with mitochondrial damage

(A) Mitochondrial structure in podocytes of db/db and DIO mice showed by TEM (n = 3) (scale bars, 0.3μm).

(B) Mitochondrial oxygen consumption ratio (OCR) of MPC5 cells treated with 0.25 mM PA for 8 h (n = 8).

(C) Mitochondrial structure of PA-treated MPC5 cells showed by TEM (n = 5) (scale bars, 0.6μm).

(D) Autophagosomes in PA-treated MPC5 cells showed by TEM (n = 5) (scale bars, 1.2μm). Data are mean ± SEM *p < 0.05, **p < 0.01, ***p < 0.001 with Student's *t* test.

(West et al., 2015). Using transmission electron microscopy (TEM), we found macropores in the mitochondrial membrane and blurry mitochondrial cristae in podocytes of db/db mice and DIO mice (Figure 6A). In cultured MPC5 podocytes, PA treatment decreased basal and maximal mitochondrial respiration rates and impaired ATP production (Figure 6B), which was accompanied by mitochondrial structural disruption and the appearance of vacuoles in the stroma (Figure 6C). As PA concentrations increased, the number of autophagosomes showed a reduction (Figure 6D). It is possible that autophagy is oversaturated in the presence of severe mitochondrial damages, causing the accumulation of damaged mitochondria. These results suggest that lipotoxicity-induced cGAS-STING activation in podocytes is accompanied by mitochondrial damage and dysfunction.

Cytosolic mtDNA activates cyclic GMP-AMP synthase-stimulator of interferon gene in podocytes upon lipotoxicity

Given the damaged mitochondrial structure, we speculated that the mtDNA leakage into the cytosol activates the cGAS-STING pathway. To address whether the cytosolic mtDNA is required for cGAS-STING activation, we depleted mtDNA in MPC5 cells by ethidium bromide (EtBr) treatment. EtBr blocks the replication and transcription of mtDNA but not nuclear DNA at low concentrations (0.1-2 mg/mL) (Hashiguchi and Zhang-Akiyama, 2009) and has been shown to block most PA-induced events, including reduced nephrin and podocin protein levels (Figures 7A and 7B), apoptosis (Figures 7A-7D), increased inflammatory cytokines (Figure 7E). Likewise, PA-induced increases in cGAS and STING proteins, as well as the phosphorylation of TBK1 and NF-kB p65, were abolished by EtBr (Figures 7F and 7G). Of note, EtBr improved mitochondrial function and morphology in the presence of PA, but showed adverse effects in the absence of PA (Figures 7H and 7I). It is conceivable that EtBr-mediated inhibition of mtDNA replication and transcription

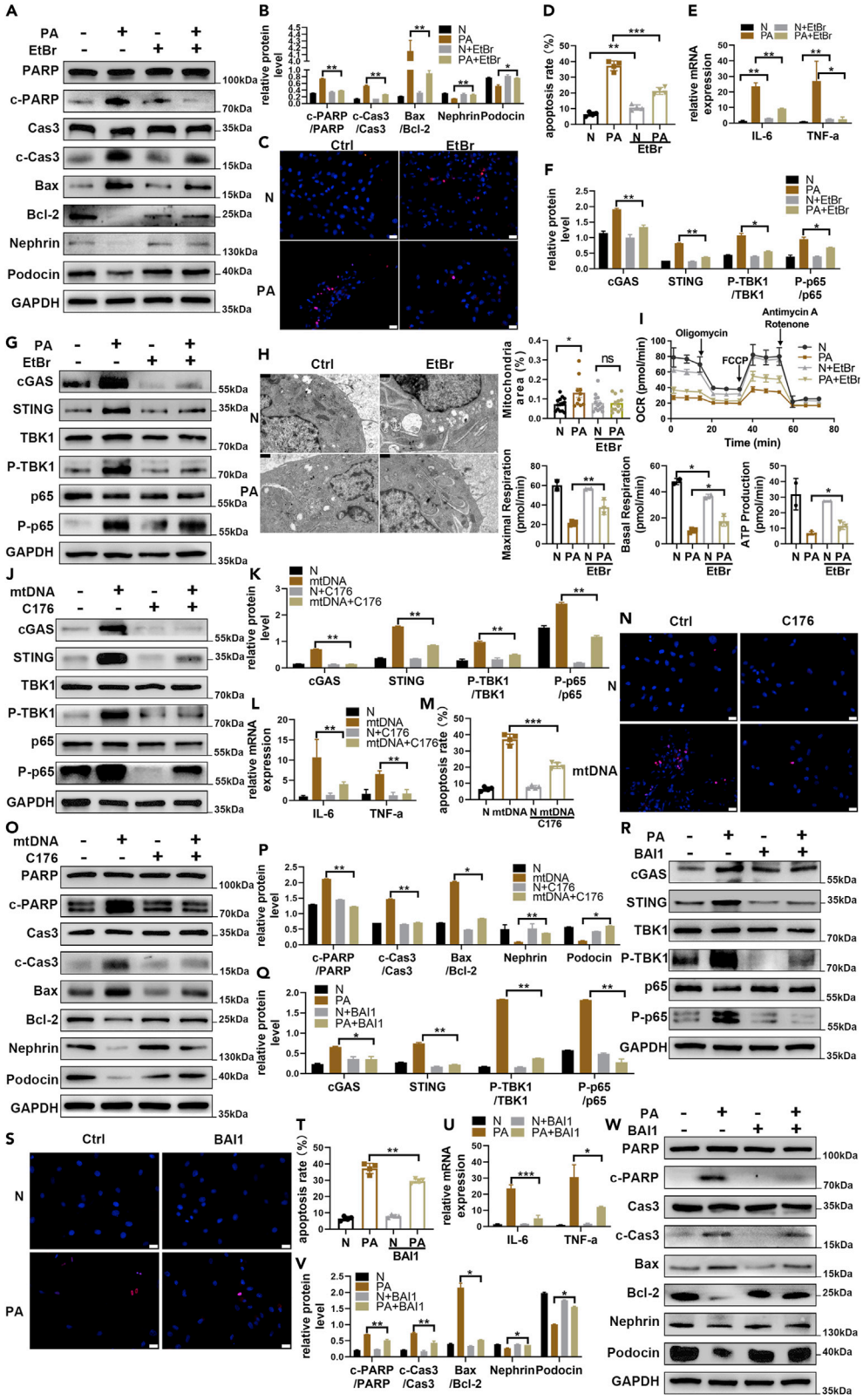
A
PA
EtBr
PARP
c-PARP
Cas3
c-Cas3
Bax
Bcl-2
Nephrin
Podocin
GAPDH
100kDa
70kDa
35kDa
15kDa
25kDa
130kDa
40kDa
B
relative protein level
c-PARP /PARP
c-Cas3 /Cas3
Bax /Bcl-2
Nephrin
Podocin
N
PA
N+EtBr
PA+EtBr
C
Ctrl
EtBr
N
PA
D
apoptosis rate (%)
E
relative mRNA expression
IL-6
TNF-a
F
cGAS
STING
P-TBK1 /TBK1
P-p65 /p65
G
cGAS
STING
TBK1
P-TBK1
p65
P-p65
GAPDH
55kDa
35kDa
70kDa
H
Ctrl
EtBr
Mitochondria area (%)
ns
I
Oligomycin
Antimycin A
Rotenone
FCCP
OCR (pmol/min)
Time (min)
Maximal Respiration (pmol/min)
Basal Respiration (pmol/min)
ATP Production (pmol/min)
J
mtDNA
C176
K
mtDNA
N+C176
mtDNA+C176
L
M
N
Ctrl
C176
O
P
Q
R
BAI1
N+BAI1
PA+BAI1
S
T
U
V
W

Figure 7. Cytosolic mtDNA activates cGAS-STING in podocytes upon lipotoxicity

(A and B) Western blot analysis of Bax/Bcl2, c-Cas3/Cas3, c-PARP/PARP, nephrin, and podocin in EtBr-treated (1.0 mg/mL) MPC5 cells (n = 6).

(C and D) TUNEL staining of EtBr-treated MPC5 cells following PA treatment (n = 4) (scale bars, 20μm).

(E) RT-qPCR analysis of mRNA levels of IL-6 and TNF-α (n = 6).

(F and G) Western blot analysis of cGAS, STING, P-TBK1/TBK1, and P-p65/p65 in EtBr-treated MPC5 cells following PA treatment (n = 6).

(H) Mitochondrial structure and area statistics in EtBr-treated MPC5 cells by TEM (n = 4) (scale bars, 0.6μm).

(I) Mitochondrial oxygen consumption ratio (OCR) of EtBr-treated MPC5 cells (n = 8).

(J and K) Western blot analysis of cGAS, STING, P-TBK1/TBK1, and P-p65/p65 after mtDNA transfection (n = 5).

(L) RT-qPCR analysis of mRNA levels of IL-6 and TNF-α in MPC5 cells after mtDNA transfection (n = 5).

(M and N) TUNEL staining of MPC5 cells following mtDNA transfection (n = 4).

(O and P) Western blot analysis of Bax/Bcl2, c-Cas3/Cas3, c-PARP/PARP, nephrin, and podocin after mtDNA transfection (2.5 mg/well) for 24 h (n = 5).

(Q and R) Western blot analysis of cGAS, STING, P-TBK1/TBK1, and P-p65/p65 in BAI1-treated MPC5 cells (n = 5).

(S and T) TUNEL staining of BAI1-treated MPC5 cells following PA treatment (n = 4) (scale bars, 20μm).

(U) RT-qPCR analysis of mRNA levels of IL-6 and TNF-α in BAI1-treated MPC5 cells (n = 6).

(V and W) Western blot analysis of Bax/Bcl2, c-Cas3/Cas3, c-PARP/PARP, nephrin, and podocin in BAI1-treated (5 μM) MPC5 cells (n = 5). Data are mean ± SEM *p < 0.05, **p < 0.01, ***p < 0.001 with Kruskal-Wallis test. Sample size is as indicated in the graphs unless otherwise described. See also Figure S7.

could compromise mitochondrial functions under baseline conditions. However, in the presence of PA, the beneficial effect of EtBr in suppressing cGAS-STING activation prevails and results in a net improvement.

To further address whether cGAS-STING can be activated by cytosolic mtDNA, we transfected MPC5 cells with isolated mtDNA. The transfected cytosolic mtDNA induced STING activation, as shown by TBK1 and NF-kB p65 phosphorylation (Figures 7J and 7K). Importantly, such artificial activation of the cGAS-STING pathway in the absence of lipotoxicity or metabolic stress is sufficient to increase the production of inflammatory cytokines (Figure 7L), decrease nephrin and podocin protein levels, and cause podocyte apoptosis (Figures 7M–7P). These adverse effects were markedly attenuated by C176 (Figures 7J-7P), which demonstrated that the cytotoxic effects are owing to the activation of the cGAS-STING pathway, not other non-specific effects of cytosolic mtDNA.

There are several possible mechanisms by which mtDNA leaks into the cytosol to induce the cGAS-STING pathway. BAX-mediated pores in the mitochondrial outer membrane allow the inner membrane to herniate, leaking mitochondrial matrix components such as mtDNA (McArthur et al., 2018). We found PA increased the protein level of BAX in MPC5 cells. Therefore, we used BAI1, an inhibitor of BAX, to evaluate the contribution of BAX to the leakage of mtDNA into the cytosol. BAI1 blocked PA-induced activation of cGAS-STING, as evidenced by decreased TBK1 and NF-kB p65 phosphorylation (Figures 7Q and 7R). BAI1 attenuated PA-induced podocyte injury as evidenced by restored protein level of nephrin and podocin, reduced apoptosis, and reduced the production of inflammatory cytokines (Figures 7S-7W). Specific knockdown of BAX by siRNA produced similar results (Figures S7A-S7C). We also performed the inhibition of the mitochondrial permeability transition pore (mPTP) by cyclosporin A (CsA) in MPC5 cells to address alternate pathways. Pretreatment of MPC5 with CsA (12.5 μM) before PA stimulation did not alter the activation of the cGAS-STING pathway, suggesting that the inhibition of mPTP opening is not sufficient to inhibit cGAS-STING activation and the mtDNA efflux does not require mPTP opening (Figure S7D). Our results suggest that the BAX macropores are the major mechanism that mediates mtDNA efflux in podocytes in the presence of lipotoxicity. Taken together, these data demonstrated that BAX-mediated mtDNA leakage into the cytosol and the subsequent activation of the cGAS-STING pathway is sufficient to cause podocyte injury in the absence of lipotoxicity and required for podocyte injury in the presence of lipotoxicity.

DISCUSSION

In the present study, we find that lipotoxicity, obesity, or diabetes causes mitochondrial dysfunction and damage in kidney podocytes, which leads to mtDNA leakage to the cytosol through BAX-mediated macropore mechanisms. Cytosolic mtDNA then activates the cGAS-STING/TBK1/p65 pathway, but not the cGAS-STING/TBK1/IRF3 pathway, which leads to inflammatory cytokine production and podocyte injury. Our findings are in agreement with mtDNA cytosolic leakage as a danger-associated molecular pattern (DAMP) to trigger immune responses (Harding et al., 2017) under pathophysiologic conditions such as NAFLD (Luo et al., 2018; Yu et al., 2019), myocardial infarction-related inflammation (Rech and Rainer,

2021), and acute kidney injury (Maekawa et al., 2019). Therefore, the mtDNA-cGAS-STING axis seems to be a common pathway for chronic inflammation (Bai and Liu, 2019).

Innate immune responses to infectious agents are usually self-limiting. The activation of the cGAS-STING pathway is associated with the degradation of STING protein (Gonugunta et al., 2017). However, we found that the protein levels of cGAS and STING were increased in the renal cortex in the presence of obesity or in PA-treated MPC5 podocytes when the cGAS-STING pathway was activated. Consistent with our results, the activation of the cGAS-STING pathway is accompanied by an increased protein level of STING under metabolic disruptions. For example, the protein level of STING is increased in the liver of human subjects with NAFLD (Luo et al., 2018) or NASH (Wang et al., 2020). The protein level of STING is also upregulated in the liver (Qiao et al., 2018) and myocardium of obese mice (Ma et al., 2022) or in the kidney of mice after cisplatin treatment (Maekawa et al., 2019). We speculate that obesity or metabolic disruption activates cGAS-STING differently from infectious agents. STING protein contains a motif (helix aa281-297) with two patches of negatively charged surface residuals (E281/D282 and E296/D297) that, when mutated, delays STING protein degradation. Mutations of the region (R281Q and R284G) are associated with an autoinflammatory disease known as STING-associated vasculopathy with onset in infancy (SAVI) (Gonugunta et al., 2017). It is unknown whether and how STING protein degradation contributes to the chronic activation of STING signaling in obese conditions. One possibility is that, under obesity or metabolic disruption, endolysosomes, the STING protein degradation becomes dysregulated, leading to impaired STING degradation and elevated STING protein level. Further studies are needed to explore the underpinning mechanisms.

We found that STING and cGAS protein levels were upregulated at 4 weeks while the downstream TBK1 was not activated at this point. It suggests that the downstream TBK1 activation is not entirely dependent on the cGAS/STING protein level elevation, although the magnitude and kinetics of the upstream STING signal can differ from downstream responses (Gulen et al., 2017).

It is known that STING affects type I IFN and proinflammatory genes through IRF3 and NF-κB pathways (Paludan and Bowie, 2013). However, we found that the activation of the cGAS-STING pathway in the renal cortex in the presence of obesity or in PA-treated MPC5 podocytes is associated with TBK1 and p65 phosphorylation, but not IRF3 phosphorylation or expression of type 1 IFNs. It is unclear what caused such a selective activation of downstream effectors and its physiological significance. Consistent with our results, previous studies also found that the phosphorylation of IRF3 is absent in renal tubular cells in acute kidney injury (Maekawa et al., 2019; Chung et al., 2019). In the Kupffer cells of the liver, lipid overload activates STING/TBK1/NF-κB pathway in non-alcoholic steatohepatitis but not the STING/TBK1/IRF3 pathway (Yu et al., 2019). In hepatocytes, lipid overload activates both STING/TBK1/NF-κB and STING/TBK1/IRF3 pathway in non-alcoholic fatty liver disease (Li and Su, 2020), but ethanol activates STING/TBK1/IRF3 in alcoholic liver disease without the involvement of inflammation (Petrasek et al., 2013). In the STING oligomer, some of the C-terminal tails (CTT) recruit TBK1, which in turn phosphorylates the CTT domain of STING, leading to the recruitment of IRF3 for phosphorylation by TBK1 (Margolis et al., 2017; Zhang et al., 2019). The CTT region of STING is essential for IRF3 activation and type I IFN production following STING activation (Tanaka and Chen, 2012). The STING S365A mutation abrogates IRF3 binding and type I interferon induction, but retains the ability to recruit TBK1 and activate NF-κB. In contrast, the STING L373A mutation or C-terminal tail truncation disrupts TBK1 binding and therefore prevents the activation of both IRF3 and NF-κB. Therefore, the activation of IRF3 and p65 by TBK1 can be independently regulated. In addition to alterations of STING in protein structure, studies have also found caspases attenuate the subsequent cGAS/STING-mediated interferon response by driving rapid cellular collapse and clearance (White et al., 2014). The exact molecular mechanism and the physiological significance warrant further investigation.

We demonstrated the activation of the cGAS-STING pathway in podocytes in db/db mice and DIO mice. Pharmacological inhibition of the STING or its downstream effector TBK1 ameliorated podocyte injury in these mouse models. The nephroprotective effect of STING/TBK1 inhibition is not simply owing to their alleviation of obesity or systemic metabolism because (1) C176 alleviated kidney injury in db/db mice without robustly improving hyperglycemia, dyslipidemia, or obesity; (2) the nephroprotective effect of C176 preceded its beneficial effect on glucose levels in DIO mice; and (3) the effects of C176 or genetic STING knockdown are cell-autonomous in cultured podocytes. In summary, these findings provide a proof-of-concept that the cGAS-STING pathway is a potential therapeutic target for preventing or treating DKD and other obesity-related kidney diseases.

Limitations of the study

We did not generate podocyte-specific STING knockout mice and cannot completely exclude the effect of improved systemic metabolism on podocyte function. And we did not perform observations in mice with advanced diabetic nephropathy so as to explore whether the inhibition of the cGAS-STING signaling pathway plays a role in advanced diabetic nephropathy.

STAR★METHODS

Detailed methods are provided in the online version of this paper and include the following:

- KEY RESOURCES TABLE
- RESOURCE AVAILABILITY
  - Lead contact
  - Materials availability
  - Data and code availability
- EXPERIMENTAL MODEL AND SUBJECT DETAILS
  - Animals
  - Cell line
- METHOD DETAILS
  - Body composition, metabolites, and metabolic testing
  - Histology and transmission electron microscopy (TEM)
  - Cell transfection and calorimetry
  - Western blotting and quantitative real-time PCR
- QUANTIFICATION AND STATISTICAL ANALYSIS

SUPPLEMENTAL INFORMATION

Supplemental information can be found online at https://doi.org/10.1016/j.isci.2022.105145.

ACKNOWLEDGMENTS

This work was supported by the National Natural Science Foundation of China (grant numbers 81770818, 81800727), the Taishan Scholar Foundation of Shandong Province (ts201712089), and the Natural Science Foundation of Shandong Province (ZR2019BH018).

AUTHOR CONTRIBUTIONS

N.Z. and C.W. conceived the study and designed experiments. N.Z., C.C., J.S., and M.X. conducted experiments. N.Z., H.H, M.Y., and Q.H. analyzed the data. N.Z., Z.S., and X.G. interpreted the data. C.W., L.C., L.W., and X.H. acquired funding. N.Z. and Z.S. wrote the article with input from other authors.

DECLARATION OF INTERESTS

The authors declare no competing interests.

Received: January 25, 2022
Revised: August 25, 2022
Accepted: September 12, 2022
Published: October 21, 2022

REFERENCES

Bai, J., and Liu, F. (2019). The cGAS-cGAMP-STING pathway: a molecular link between immunity and metabolism. Diabetes *68*, 1099–1108. https://doi.org/10.2337/dbi18-0052.

Chen, Q., Sun, L., and Chen, Z.J. (2016). Regulation and function of the cGAS-STING pathway of cytosolic DNA sensing. Nat. Immunol. *17*, 1142–1149. https://doi.org/10.1038/ni.3558.

Chung, K.W., Dhillon, P., Huang, S., Sheng, X., Shrestha, R., Qiu, C., Kaufman, B.A., Park, J., Pei, L., Baur, J., et al. (2019). Mitochondrial damage and activation of the STING pathway lead to renal inflammation and fibrosis. Cell Metab. *30*, 784–799.e5. https://doi.org/10.1016/j.cmet.2019.08.003.

Dai, H., Liu, Q., and Liu, B. (2017). Research progress on mechanism of podocyte depletion in diabetic nephropathy. J. Diabetes Res. *2017*, 2615286. https://doi.org/10.1155/2017/2615286.

Gonugunta, V.K., Sakai, T., Pokatayev, V., Yang, K., Wu, J., Dobbs, N., and Yan, N. (2017). Trafficking-mediated STING degradation requires sorting to acidified endolysosomes and can Be targeted to enhance anti-tumor response. Cell Rep. *21*, 3234–3242. https://doi.org/10.1016/j.celrep.2017.11.061.

Greka, A., and Mundel, P. (2012). Cell biology and pathology of podocytes. Annu. Rev. Physiol. *74*, 299–323. https://doi.org/10.1146/annurev-physiol-020911-153238.

Gulen, M.F., Koch, U., Haag, S.M., Schuler, F., Apetoh, L., Villunger, A., Radtke, F., and Ablasser, A. (2017). Signalling strength determines proapoptotic functions of STING. Nat. Commun. *8*, 427. https://doi.org/10.1038/s41467-017-00573-w.

Harding, S.M., Benci, J.L., Irianto, J., Discher, D.E., Minn, A.J., and Greenberg, R.A. (2017). Mitotic progression following DNA damage enables pattern recognition within micronuclei. Nature *548*, 466–470. https://doi.org/10.1038/nature23470.

Hashiguchi, K., and Zhang-Akiyama, Q.M. (2009). Establishment of human cell lines lacking mitochondrial DNA. Methods Mol. Biol. *554*, 383–391. https://doi.org/10.1007/978-1-59745-521-3_23.

Hickey, F.B., and Martin, F. (2018). Role of the immune system in diabetic kidney disease. Curr. Diab. Rep. *18*, 20. https://doi.org/10.1007/s11892-018-0984-6.

Li, Y.N., and Su, Y. (2020). Remdesivir attenuates high fat diet (HFD)-induced NAFLD by regulating hepatocyte dyslipidemia and inflammation via the suppression of STING. Biochem. Biophys. Res. Commun. *526*, 381–388. https://doi.org/10.1016/j.bbrc.2020.03.034.

Luo, X., Li, H., Ma, L., Zhou, J., Guo, X., Woo, S.L., Pei, Y., Knight, L.R., Deveau, M., Chen, Y., et al. (2018). Expression of STING is increased in liver tissues from patients with NAFLD and promotes macrophage-mediated hepatic inflammation and fibrosis in mice. Gastroenterology *155*, 1971–1984.e4. https://doi.org/10.1053/j.gastro.2018.09.010.

Ma, X.M., Geng, K., Law, B.Y.K., Wang, P., Pu, Y.L., Chen, Q., Xu, H.W., Tan, X.Z., Jiang, Z.Z., and Xu, Y. (2022). Lipotoxicity-induced mtDNA release promotes diabetic cardiomyopathy by activating the cGAS-STING pathway in obesity-related diabetes. Cell Biol. Toxicol. https://doi.org/10.1007/s10565-021-09692-z.

Maekawa, H., Inoue, T., Ouchi, H., Jao, T.M., Inoue, R., Nishi, H., Fujii, R., Ishidate, F., Tanaka, T., Tanaka, Y., et al. (2019). Mitochondrial damage causes inflammation via cGAS-STING signaling in acute kidney injury. Cell Rep. *29*, 1261–1273.e6. https://doi.org/10.1016/j.celrep.2019.09.050.

Margolis, S.R., Wilson, S.C., and Vance, R.E. (2017). Evolutionary origins of cGAS-STING signaling. Trends Immunol. *38*, 733–743. https://doi.org/10.1016/j.it.2017.03.004.

McArthur, K., Whitehead, L.W., Heddleston, J.M., Li, L., Padman, B.S., Oorschot, V., Geoghegan, N.D., Chappaz, S., Davidson, S., San Chin, H., et al. (2018). BAK/BAX macropores facilitate mitochondrial herniation and mtDNA efflux during apoptosis. Science *359*, eaao6047. https://doi.org/10.1126/science.aao6047.

Menini, S., Iacobini, C., Oddi, G., Ricci, C., Simonelli, P., Fallucca, S., Grattarola, M., Pugliese, F., Pesce, C., and Pugliese, G. (2007). Increased glomerular cell (podocyte) apoptosis in rats with streptozotocin-induced diabetes mellitus: role in the development of diabetic glomerular disease. Diabetologia *50*, 2591–2599. https://doi.org/10.1007/s00125-007-0821-y.

Najafian, B., Alpers, C.E., and Fogo, A.B. (2011). Pathology of human diabetic nephropathy. Contrib. Nephrol. *170*, 36–47. https://doi.org/10.1159/000324942.

Navarro-Gonzalez, J.F., Mora-Fernández, C., Muros De Fuentes, M., and García-Pérez, J. (2011). Inflammatory molecules and pathways in the pathogenesis of diabetic nephropathy. Nat. Rev. Nephrol. *7*, 327–340. https://doi.org/10.1038/nrneph.2011.51.

Paludan, S.R., and Bowie, A.G. (2013). Immune sensing of DNA. Immunity *38*, 870–880. https://doi.org/10.1016/j.immuni.2013.05.004.

Pavenstadt, H., Kriz, W., and Kretzler, M. (2003). Cell biology of the glomerular podocyte. Physiol. Rev. *83*, 253–307. https://doi.org/10.1152/physrev.00020.2002.

Perkins, B.A., Ficociello, L.H., Silva, K.H., Finkelstein, D.M., Warram, J.H., and Krolewski, A.S. (2003). Regression of microalbuminuria in type 1 diabetes. N. Engl. J. Med. *348*, 2285–2293. https://doi.org/10.1056/NEJMoa021835.

Petrasek, J., Iracheta-Vellve, A., Csak, T., Satishchandran, A., Kodys, K., Kurt-Jones, E.A., Fitzgerald, K.A., and Szabo, G. (2013). STING-IRF3 pathway links endoplasmic reticulum stress with hepatocyte apoptosis in early alcoholic liver disease. Proc. Natl. Acad. Sci. USA *110*, 16544–16549. https://doi.org/10.1073/pnas.1308331110.

Qiao, J.T., Cui, C., Qing, L., Wang, L.S., He, T.Y., Yan, F., Liu, F.Q., Shen, Y.H., Hou, X.G., and Chen, L. (2018). Activation of the STING-IRF3 pathway promotes hepatocyte inflammation, apoptosis and induces metabolic disorders in nonalcoholic fatty liver disease. Metabolism *81*, 13–24. https://doi.org/10.1016/j.metabol.2017.09.010.

Rech, L., and Rainer, P.P. (2021). The innate immune cGAS-STING-pathway in cardiovascular diseases - a mini review. Front. Cardiovasc. Med. *8*, 715903. https://doi.org/10.3389/fcvm.2021.715903.

Rumora, A.E., Lentz, S.I., Hinder, L.M., Jackson, S.W., Valesano, A., Levinson, G.E., and Feldman, E.L. (2018). Dyslipidemia impairs mitochondrial trafficking and function in sensory neurons. FASEB J. *32*, 195–207. https://doi.org/10.1096/fj.201700206R.

Schindelin, J., Arganda-Carreras, I., Frise, E., Kaynig, V., Longair, M., Pietzsch, T., Preibisch, S., Rueden, C., Saalfeld, S., Schmid, B., et al. (2012). Fiji: an open-source platform for biological-image analysis. Nat. Methods *9*, 676–682. https://doi.org/10.1038/nmeth.2019.

Sieber, J., Lindenmeyer, M.T., Kampe, K., Campbell, K.N., Cohen, C.D., Hopfer, H., Mundel, P., and Jehle, A.W. (2010). Regulation of podocyte survival and endoplasmic reticulum stress by fatty acids. Am. J. Physiol. Renal Physiol. *299*, F821–F829. https://doi.org/10.1152/ajprenal.00196.2010.

Sieber, J., Weins, A., Kampe, K., Gruber, S., Lindenmeyer, M.T., Cohen, C.D., Orellana, J.M., Mundel, P., and Jehle, A.W. (2013). Susceptibility of podocytes to palmitic acid is regulated by stearoyl-CoA desaturases 1 and 2. Am. J. Pathol. *183*, 735–744. https://doi.org/10.1016/j.ajpath.2013.05.023.

Sun, Y., Cui, S., Hou, Y., and Yi, F. (2021). The updates of podocyte lipid metabolism in proteinuric kidney disease. Kidney Dis. *7*, 438–451. https://doi.org/10.1159/000518132.

Tanaka, Y., and Chen, Z.J. (2012). STING specifies IRF3 phosphorylation by TBK1 in the cytosolic DNA signaling pathway. Sci. Signal. *5*, ra20. https://doi.org/10.1126/scisignal.2002521.

Thomson, D.W., Poeckel, D., Zinn, N., Rau, C., Strohmer, K., Wagner, A.J., Graves, A.P., Perrin, J., Bantscheff, M., Duempelfeld, B., et al. (2019). Discovery of GSK8612, a highly selective and potent TBK1 inhibitor. ACS Med. Chem. Lett. *10*, 780–785. https://doi.org/10.1021/acsmedchemlett.9b00027.

Van Buren, P.N., and Toto, R. (2013). Current update in the management of diabetic nephropathy. Curr. Diabetes Rev. *9*, 62–77.

Wang, X., Rao, H., Zhao, J., Wee, A., Li, X., Fei, R., Huang, R., Wu, C., Liu, F., and Wei, L. (2020). STING expression in monocyte-derived macrophages is associated with the progression of liver inflammation and fibrosis in patients with nonalcoholic fatty liver disease. Lab. Invest. *100*, 542–552. https://doi.org/10.1038/s41374-019-0342-6.

West, A.P., Khoury-Hanold, W., Staron, M., Tal, M.C., Pineda, C.M., Lang, S.M., Bestwick, M., Duguay, B.A., Raimundo, N., Macduff, D.A., et al. (2015). Mitochondrial DNA stress primes the antiviral innate immune response. Nature *520*, 553–557. https://doi.org/10.1038/nature14156.

White, M.J., Mcarthur, K., Metcalf, D., Lane, R.M., Cambier, J.C., Herold, M.J., van Delft, M.F., Bedoui, S., Lessene, G., Ritchie, M.E., et al. (2014). Apoptotic caspases suppress mtDNA-induced STING-mediated type I IFN production. Cell *159*, 1549–1562. https://doi.org/10.1016/j.cell.2014.11.036.

Yu, Y., Liu, Y., An, W., Song, J., Zhang, Y., and Zhao, X. (2019). STING-mediated inflammation in Kupffer cells contributes to progression of nonalcoholic steatohepatitis. J. Clin. Invest. *129*, 546–555. https://doi.org/10.1172/JCI121842.

Zhang, C., Shang, G., Gui, X., Zhang, X., Bai, X.C., and Chen, Z.J. (2019). Structural basis of STING binding with and phosphorylation by TBK1. Nature *567*, 394–398. https://doi.org/10.1038/s41586-019-1000-2.

Zhang, X., Wu, J., Du, F., Xu, H., Sun, L., Chen, Z., Brautigam, C.A., Zhang, X., and Chen, Z.J. (2014). The cytosolic DNA sensor cGAS forms an oligomeric complex with DNA and undergoes switch-like conformational changes in the activation loop. Cell Rep. *6*, 421–430. https://doi.org/10.1016/j.celrep.2014.01.003.

Zhao, P., Wong, K.I., Sun, X., Reilly, S.M., Uhm, M., Liao, Z., Skorobogatko, Y., and Saltiel, A.R. (2018). TBK1 at the crossroads of inflammation and energy homeostasis in adipose tissue. Cell *172*, 731–743.e12. https://doi.org/10.1016/j.cell.2018.01.007.

Ziyadeh, F.N. (2004). Mediators of diabetic renal disease: the case for tgf-Beta as the major mediator. J. Am. Soc. Nephrol. *15*, S55–S57. https://doi.org/10.1097/01.asn.0000093460.24823.5b.

Ziyadeh, F.N., Hoffman, B.B., Han, D.C., Iglesias-De La Cruz, M.C., Hong, S.W., Isono, M., Chen, S., Mcgowan, T.A., and Sharma, K. (2000). Long-term prevention of renal insufficiency, excess matrix gene expression, and glomerular mesangial matrix expansion by treatment with monoclonal antitransforming growth factor-beta antibody in db/db diabetic mice. Proc. Natl. Acad. Sci. USA *97*, 8015–8020. https://doi.org/10.1073/pnas.120055097.

STAR★METHODS

KEY RESOURCES TABLE

REAGENT or RESOURCE	SOURCE	IDENTIFIER
Antibodies		
Anti-cGAS	CST	Cat#31659S; RRID: AB_2799008
Anti-STING	Protech	Cat#19851-1-AP; RRID: AB_10665370
Anti-STING	CST	Cat#50494S; RRID: AB_2799375
Anti-TBK1	CST	Cat#3504T; RRID: AB_2255663
Anti phospho-TBK1	CST	Cat#5483S; RRID: AB_10693472
Anti-IRF3	Protech	Cat#11312-1-AP; RRID: AB_2127004
Anti-Phospho-IRF3	CST	Cat#29047S; RRID: AB_2773013
Anti-NF-kB p65	CST	Cat#8242T; RRID: AB_10859369
Anti-Phospho-p65	CST	Cat#3033T; RRID: AB_331284
Anti-IFN-β	BIOSS	Cat#bs-23733R
Anti-Bax	Abcam	Cat#ab32503; RRID: AB_725631
Anti-Bcl-2	Abcam	Cat#ab32124; RRID: AB_725644
Anti-Caspase-3	CST	Cat#9662; RRID: AB_331439
Anti-Cleaved-caspase3	CST	Cat#9664; RRID: AB_2070042
Anti-PARP	CST	Cat#9542; RRID: AB_2160739
Anti-Cleaved-PARP	CST	Cat#9548; RRID: AB_2160592
Anti-Podocin	Bioss	Cat#bs-6597R; RRID: AB_11103353
Anti-Nephrin	Bioss	Cat#bs-4866R
Anti-Nephrin	Santa Cruz	Cat#sc-377246
Anti-synaptopodin	Protech	Cat#21064-1-AP; RRID: AB_10733120
Anti-WT-1	Millipore	Cat#MAB4234; AB_570945
Anti-GM130	BD Biosciences	Cat#610823; RRID: AB_398142
Anti-GAPDH	Protech	Cat#60004-1-Ig; RRID: AB_2107436
Chemicals, peptides, and recombinant proteins		
high-glucose Dulbecco's modified Eagle's medium	Gibco	Cat#C12430500BT
RIPA	Beyotime	Cat#P0013B
Lipofectamine2000	Invitrogen	Cat#11668019
Lipofectamine3000	Invitrogen	Cat#L3000015
RNAiso Plus	Takara	Cat#D9108A
palmitic acid	Sigma-Aldrich	Cat#P5585
Seahorse XF DMEM Medium	Agilent	Cat#103575–100
Seahorse XF Glucose	Agilent	Cat#103577-100
Seahorse XF Pyruvate	Agilent	Cat#103578-100
Seahorse XF Glutamine	Agilent	Cat#103579-100
C-176	Selleck	Cat#314054-00-7
GSK8612	Selleck	Cat#2361659-62-1
BAI1	Selleck	Cat#335165-68-9
Cyclosporin A	Selleck	Cat#59865-13-3
EtBr	Selleck	Cat#1239-45-8

(*Continued on next page*)

Continued

REAGENT or RESOURCE	SOURCE	IDENTIFIER
Critical commercial assays		
Microalbumin Assay Kit	Nanjing Jiancheng Bioengineering Institute	Cat#H127-1-2
Glycogen Periodic Acid Schiff (PAS/Hematoxylin) Stain Kit	Solarbio	Cat#G1281
Modified Masson's Trichrome Stain Kit	Solarbio	Cat#G1346
TMR (red) Tunel Cell Apoptosis Detection Kit	Servicebio	Cat#G1502-100T
DAB (SA-HRP) Tunel Cell Apoptosis Detection Kit	Servicebio	Cat#G1507-100T
Mitochondrial DNA Isolation Kit	Abcam	Cat#ab65321
PrimeScriptTM II Reverse Transcriptase	Takara	Cat#RR047
SYBR Green PCR kit	Takara	Cat#RR820
XF Cell Mito Stress Test Kit	Agilent	Cat#103015-100
Experimental models: Cell lines		
conditionally immortalized mouse podocytes	ATCC	RRID: CVCL_AS87
Experimental models: Organisms/strains		
Mouse: *C57BL/6J*	Charles River	N/A
Mouse: BKS.Cg-Dock7m+/+ Leprdb/J	Charles River	N/A
Oligonucleotides		
siRNA targeting sequence of STING; 5′-CCAUGU CACAGGAUGGCAATT-3′, 5′-UUGCCAUCCUG UGACAUGGTT-3′	This paper	N/A
siRNA targeting sequence of BAX; 5′-CCAGCUC UGAACAGAUCAUTT-3′, 5′-AUGAUCUGUUCA GAGCUGGTT-3′	This paper	N/A
siRNA negative control sequence; 5′-UUCUC CGAACGUGUCACGUTT-3′′and 5′-ACGUG ACACGUUCGGAGAATT-3′	This paper	N/A
Forward primer for mouse β-actin; 5′-ACCG TGAAAAGATGACCCAG-3′	This paper	N/A
Reverse primer for mouse β-actin; 5′-GTACG ACCAGAGGCATACAG-3′	This paper	N/A
Forward primer for mouse IL-6; 5′-CAGAGGA TACCACTCCCAAC-3′	This paper	N/A
Reverse primer for mouse IL-6; 5′-CAATCAG AATTGCCATTGCC-3′	This paper	N/A
Forward primer for mouse TNF-α; 5′-GTTGTA CCTTGTCTACTCCCAG-3′	This paper	N/A
Reverse primer for mouse TNF-α; 5′-GGTTGA CTTTCTCCTGGTATGAG-3′	This paper	N/A
Software and algorithms		
Prism 6 software	GraphPad Inc.	https://www.graphpad.com
FIJI software	Schindelin et al., 2012	https://imagej.nih.gov/ij/
Seahorse Wave Desktop	Agilent	https://www.agilent.com.cn

RESOURCE AVAILABILITY

Lead contact

Further information and requests for resources and reagents should be directed to and will be fulfilled by the lead contact, Nan Zang (632560877@qq.com).

Materials availability

This study did not generate new unique reagents.

Data and code availability

All data reported in this paper will be shared by the lead contact upon request. This paper does not report original code. Any additional information required to reanalyze the data reported in this paper is available from the lead contact upon request.

EXPERIMENTAL MODEL AND SUBJECT DETAILS

Animals

Animal experiments were approved by the Animal Care and Use Committee of Shandong University. Mice were maintained under a 12-h light/dark cycle at room temperature (22–25°C) and humidity 55 ± 5% with *ad libitum* access to water and a standard laboratory diet. Water and cages were autoclaved, and no mice became severely ill until the end of the experiments. For all the mice experiments, mice were randomly assigned to experimental groups. Fifteen male diabetic db/db mice (Strain: BKS.Cg-Dock7m+/+ Leprdb/J), a widely-used diabetes/obesity mouse model, and fourteen lean, nondiabetic db/m littermate control mice at approximately 4 weeks were selected for investigating the dynamic renal pathological characteristics. Body weight and fasting blood glucose (FBG) were measured weekly. Three mice were euthanized at random every two weeks to collect serum and kidney tissue. For STING inhibitors, six male db/db mice (7 weeks of age) were injected intraperitoneally with N-(4-iodophenyl)-5-nitrofuran-2-carboxamide (C-176) (5 mg/kg) or dimethyl sulfoxide (DMSO) vehicle diluted in corn oil once per day for 21 consecutive days. We repeated these experiments in a diet-induced obesity (DIO) model. After 12 weeks of high-fat diet from 6-week old, 6 male DIO mice were injected intraperitoneally with C-176 (5 mg/kg) or DMSO every other day for 4 weeks. The control mice received the same treatment. Body weight and FBG were monitored as described above.

Cell line

The MPC5 mouse podocyte line was purchased from MINGJING BIOLOGY (Shanghai, China), the agent of ATCC (USA). The cell line was cultured in the high-glucose Dulbecco's modified Eagle's medium (Gibco, USA) supplemented with 10% fetal bovine serum (Gibco, USA), 100 U/mL of penicillin and 100 μg/mL streptomycin at 37°C and 5% CO2 and was sub-cultured by 0.25% Trypsin-EDTA. The cells were photographed by inverted phase-contrast microscopy and characterized by IF of podocyte markers WT-1, synaptopodin and nephrin.

METHOD DETAILS

Body composition, metabolites, and metabolic testing

Body composition was measured using dual-energy X-ray absorptiometry (DXA). The body fat percentage refers to the percentage of the body fat mass (weight of the fat) normalized to the total body weight. Blood urea nitrogen (BUN), serum creatinine (Scr), urine albumin-to-creatinine ratio (ACR), alanine aminotransferase (ALT), aspartate transaminase (AST), triglyceride (TG), total cholesterol (TC), low-density lipoprotein cholesterol (LDL-C) and high-density lipoprotein cholesterol (HDL-C) were detected by automatic biochemical apparatus (Chemray 240 and Chemray 800). 24h urine was collected by metabolic cage to detect urinary protein. The samples were then used for ELISA tests according to the manufacturer's instructions (Jiancheng, Nanjing, China). For the intraperitoneal glucose tolerance test (IPGTT), animals were fasted for 16 h prior and received an i.p. administration of 2 g/kg glucose. The tail vein blood glucose was measured by Accu-Chek® Performa before (0min) and 30, 60, 90, 120, 150, and 180 min after the administration. For the intraperitoneal insulin tolerance test (IPITT), after a 6-h fast, mice received an i.p. administration of 0.75U/kg insulin, and the blood glucose was measured before (0min) and after the administration at 30, 60, 90, and 120 min. The area under the curve (AUC) was calculated by the trapezoidal rule.

Histology and transmission electron microscopy (TEM)

For Immunohistochemistry (IHC), after deparaffinization, antigen retrieval was performed with citrate buffer (pH = 9.0). 3% H2O2 and goat serum were used to block endogenous catalase and unspecific binding site, respectively. Primary antibodies were incubated overnight at 4°C, followed by secondary antibodies and diaminobenzidine staining according to manufacturer's instructions (BOSTER, China). For Immunofluorescence

(IF) analysis of tissue sections, antigen retrieval and blocking unspecific sites were performed before primary antibodies incubation overnight at 4°C. For IF of cells, cells were cultured on microscope cover glass overnight. After fixation in 4% paraformaldehyde and penetration in 0.1% Triton X-100, unspecific sites were blocked. Primary antibodies were incubated overnight at 4°C, followed by fluorophore-conjugated Alexa secondary antibodies (1:200, Life Technology, USA) applied at 37°C for 1 h. After 4′,6-diamidino-2-phenylindole (DAPI) staining, pictures were taken with fluorescence microscopy, and positive fluorescence areas were measured by CellSens Standard according to the manufacturer's instructions.

Hematoxylin-eosin (H&E) was performed according to the standard protocol with the reagent hematoxylin and eosin. The glomerular areas were measured by CellSens Standard. Periodic-Acid-Schiff (PAS) staining was performed according to the manufacturer's instructions (Solarbio, China). Masson (Solarbio, China) and terminal deoxynucleotidyl transferase-mediated dUTP nick-end labeling (TUNEL) staining were conducted as standard protocol according to manufacturer's instructions (Servicebio, China). For the morphological study of glomerular, each group of mice contained 4 samples, and in each sample, at least 3 sections were utilized.

Ultrastructure of podocytes was examined with TEM (JEM-1200EX). The kidney cortical tissues and conditionally immortalized mouse podocytes (MPC5) (5×10^5 cells) were fixed with 2.5% glutaraldehyde. Subsequently, the samples were washed twice with 0.1 M phosphate buffer for 30 minutes and then fixed for 2 hours with 1% OSO4, followed by dehydration through 50, 70, 80, and 90% ethanol. Specimens were embedded with the epoxy resin mixture, and the blocks were cut using an ultramicrotome. Mitochondrial area statistics are presented as the ratio of mitochondrial area to total cytoplasmic area.

Cell transfection and calorimetry

mtDNA was isolated from MPC5 cells using the Mitochondrial DNA Isolation kit according to the manufacturer's instructions (Abcam, USA). The mtDNA was precipitated with boric acid-EDTA buffer (Abcam, USA) and stored at −20°C. Cells were seeded in 6-well plates and transfected with 2.5mg/well mtDNA using Lipofectamine 3000 (Invitrogen, USA) according to the manufacturer's instructions.

For small interfering RNA (siRNA) transfection, siRNAs targeting STING (5′-CCAUGUCACAGGAUGGCAATT-3′, 5′-UUGCCAUCCUGUGACAUGGTT-3′) and negative control (NC): 5′-UUCUCCGAACGUGUCACGUTT-3′′and 5′-ACGUGACACGUUCGGAGAATT-3′ were designed and synthesized by GenePharma (Shanghai, China). siRNAs targeting BAX (5′-CCAGCUCUGAACAGAUCAUTT-3′, 5′-AUGAUCUGUUCAGAGCUGGTT-3′) and negative control (NC): 5′-UUCUCCGAACGUGUCACGUTT-3′′and 5′-ACGUGACACGUUCGGA GAATT-3′ were designed and synthesized by GenePharma (Shanghai, China). For transfection, MPC5 cells were transfected with 160 pmol siRNA using Lipofectamine 2000 Transfection Reagent (Invitrogen, USA) according to manufacturer's instructions. Cells were harvested 24 h later for RNA or 48 h for protein.

For the Seahorse experiments, the oxygen consumption ratio (OCR) was measured using an XF96 extracellular flux analyzer (Agilent Technologies) according to the procedure provided by the manufacturer. Cells were seeded at 25,000 cells per well of an XF96 cell culture microplate. OCR was assessed in a glucose-containing XF base medium (10 mM glucose, 2 mM pyruvate glutamine, and 1 mM pyruvate) according to the manufacturer's instructions. Analyses were performed using 1.5 μM oligomycin, 1 μM carbonyl cyanide-4-(trifluoromethoxy) phenylhydrazone (FCCP), and 0.5 μM antimycin A/rotenone. Data were normalized to total cell amount. Results were analyzed in WAVE software and processed through the XF Mito Stress Test Report.

Western blotting and quantitative real-time PCR

Protein levels in kidneys or cells were detected by western blotting. Total protein was extracted with lysis buffer and separated by SDS-PAGE. Subsequently, the protein was transferred onto PVDF membranes. After being blocked in 5% non-fat milk, membranes were incubated with primary antibodies at 4°C overnight. Cleaved poly ADP-ribose polymerase (PARP)/PARP, cleaved caspase 3/caspase 3, Bcl-2 associated X protein (bax)/B-cellymphoma-2 (bcl2) were used to assess apoptosis. Nephrin and Podocin were used to assess podocyte status. cGAS, STING, TBK1, P-TBK1, IRF3, P-IRF3, p65, P-p65 and IFN-β reflected activation of the cGAS-STING pathway. In the following day, membranes were incubated with a horseradish peroxidase-conjugated anti-mouse antibody (1:20,000) or anti-rabbit antibody (1:20,000) at 25°C for 1 h.

The immune complexes were visualized using enhanced chemiluminescence kit. Band intensity was quantified using FIJI software (Schindelin et al., 2012).

Total mRNA was prepared from MPC5 cells, isolated using RNAiso Plus (Takara, Japan), and was reverse transcribed using PrimeScript RT Master Mix (Takara, Japan) according to the manufacturers' instructions. The cDNA was used as the template for quantitative real-time PCR, which was performed with Fast SYBR Green Master Mix (Takara, Japan) and was programmed as follows: 5 min at 94°C, 50 cycles of 94°C for 30 s, 60°C for 30 s, and 72°C for 40 s, and a 5 s incubation at 65°C. The following primers were employed: β-actin: 5′-ACCGTGAAAAGAT GACCCAG-3′, 5′-GTACGACCAGAGGCATACAG-3′; IL-6: 5′-CAGAGGATACCACTCCCAAC-3′, 5′-CAATCA GAATTGCCATTGCC-3′; TNF-α: 5′-GTTGTACCTTGTCTACTCCCAG-3′, 5′-GGTTGACTTTCTCCTGGTAT GAG-3′

QUANTIFICATION AND STATISTICAL ANALYSIS

Data were presented as mean ± SEM and were representative of at least three independent experiments. Following the Grubbs' outlier test, differences between groups were analyze by one- or two-way analysis of variance or by the Student's t-test for experiments with only two subgroups or by Kruskal-Wallis test. $p < 0.05$ was considered statistically significant. Statistical analyses were performed using Prism 6 software. All of the statistical details of experiments can be found in the figure legends.